PERFORMANCE CHARACTERISTICS OF DIFFERENT TWO-CHANNEL GMTI DETECTORS

A. Laika [a)], F. Meyer [b)], S. Hinz [a)], S. Suchandt [b)], R. Bamler [a,b)]

[a)] Remote Sensing Technology, Technische Universitaet Müenchen
Arcisstrasse 21, D - 80333 München, Germany
[b)] Remote Sensing Technology Institute
German Aerospace Center (DLR), Oberpfaffenhofen
D - 82234 Wessling, Germany

Commission VII, Working Group VII/2

KEY WORDS: High resolution, SAR, Radar, Satellite, Monitoring, Detection, Targets

ABSTRACT:

With the amount of traffic increasing steadily, traffic monitoring has evolved to an important topic of research. Most of the conventional systems for traffic monitoring lack of spatial extent. Hence traffic monitoring from space provides an attractive alternative to supplement existing systems. The upcoming TerraSAR-X Mission with its experimental dual-receive mode will contribute to this research topic. To have an estimate on the performance of traffic monitoring achievable, simulations with respect to the TerraSAR-X instrument specifications were conducted. Simulation methods and results are presented. To complement simulations with results from SAR-Data a prototype traffic-processor is introduced and first results are shown.

1. INTRODUCTION

1.1 Motivation

As increased traffic emerges as one of the major problems in urban and sub-urban areas, traffic-monitoring has become an increasingly important research topic. Most of the conventional systems for traffic-monitoring, however, lack of spatial extent. Hence traffic monitoring from space provides an attractive alternative to supplement existing systems. One remote sensing system to think about in this context is the upcoming TerraSAR-X Mission. Its high resolution synthetic aperture radar (SAR) sensor provides the potential for new task in remote sensing. Even more importantly the sensor can also be operated in an experimental dual-receive (DRA) mode, which acquires two high resolution SAR-Images of the same scene within a small time frame. Especially this dual-receive mode is going to provide data suited for traffic monitoring.

1.2 Related Work

The task of detecting moving vehicles with SAR sensors has been addressed in several scientific publications. In military research this problem is well known as ground moving target indication (GMTI). The method of choice in GMTI is to use a SAR sensor with at least 3 channels and use space-time adaptive processing (STAP) for target detection. Further reference to that topic can be found in (Klemm, 1998). Unfortunately space borne SAR systems with 3 or more channels are currently not available. The upcoming TerraSAR-X mission is equipped with a single channel SAR that can be switched to an experimental mode with 2 channels to enable traffic monitoring. Although the use of a 2-channel system is suboptimal for detecting vehicles, some methods exist that allow detection under certain conditions. The classical method to do so is to use the displaced phase center array (DPCA) method. Along track interferometry (ATI) is another method that can be used. The issue of detecting moving targets using ATI is discussed in (Gierull, 2001). In (Gierull, 2002) special emphasis is put on the probability density functions associated with this detection. Traffic monitoring from space is quite rare so far. But as shown in (Breit *et al.* , 2003) first endeavors have already been carried out.

2. EFFECTS OF MOVING OBJECTS IN SAR IMAGES

2.1 SAR Focusing of Stationary Point Scatterers

The position of a Radar transmitter on board a satellite is given by $P_{sat}(t) = [x_{sat}(t), y_{sat}(t), z_{sat}(t)]$ with x being the along-track direction, y the across-track ground range direction and z being the vertical. A point scatterer is assumed to be at position $P_{mover} = [x_{mover}(t), y_{mover}(t), z_{mover}(t)]$. The range to an arbitrarily moving and accelerating point target from the radar platform is defined by $R(t) = P_{sat}(t) - P_{mover}(t)$ and the measured echo signal of this point scatterer can consequently be written as

$$u_s(t) = a_\theta(\theta) a_\beta(\beta) g(\tau - 2R(t)/c) \exp\{-j\frac{4\pi}{\lambda} R(t)\} \quad (1)$$

with $g(\tau - 2R(t)/c)$ being the delayed complex pulse envelope, and $a_\theta(\theta)$, $a_\beta(\beta)$ being the amplitude of the two-way antenna patterns in elevation and azimuth, respectively (Bamler and Schättler, 1993; Cumming and Wong, 2005). For further investigations the amplitude $A = a_\theta(\theta) a_\beta(\beta) g(\tau - 2R(t)/c)$ is discarded to simplify the equations. Additionally, the term $\exp\{-j\frac{4\pi}{\lambda}R(t)\}$ is approximated quadratically by $\exp\{j\pi FM t^2\}$ with:

$$FM = -\frac{2}{\lambda}\frac{d^2}{dt^2}R(t) = -\frac{2}{\lambda R} v_{sat}\, v_B \quad (2)$$

being the frequency modulation rate of the azimuth chirp, i.e.

$$u(t) = \exp\{j\pi FM t^2\} \quad (3)$$

Azimuth focussing of the SAR image is performed using the matched filter concept (Bamler and Schättler, 1993; Cumming and Wong, 2005). According to this concept the filter must correspond to

$$s(t) = \exp\{-j\pi FM t^2\} \quad (4)$$

An optimally focused image is obtained by complex-valued correlation of $u(t)$ and $s(t)$. For efficiency reasons, this operation is commonly done in frequency domain by multiplying the respective spectra $U(f)$ and $S(f)$

$$T(f) = U(f) \cdot S(f) \quad (5)$$

using highly specialized algorithms like the ω-κ algorithm or the chirp scaling algorithm (see (Cumming and Wong, 2005) for details). An important aspect refers to the definition of the matched filter. To construct it correctly, the actual range history of each target in the image must be known. For this, a priori information about sensor and scatterer position and motion is necessary. Usually, the time dependence of the scatterer position is ignored yielding $P_{mover}(t) = P_{mover}$. This concept is commonly referred to as *stationary-world matched filter* (SWMF). Because of this definition, a SWMF does not correctly represent the phase history of a significantly moving object, which eventually results in image deteriorations.

2.2 Theory of Object Motion Effects in Satellite Radar-Data

2.21 Across-track Motion The target should now move with velocity v_{y0} in across-track direction. This movement causes a change of range history proportional to the projection of the motion vector into the line-of-sight direction of the sensor $v_{los} = v_{y0} \cdot sin(\theta)$, with θ being the local elevation angle. In case of constant motion during illumination the change of range history is linear and causes an additional linear phase trend in the echo signal. The resulting signal of an object moving in line-of-sight direction with velocity v_{los} is consequently

$$u_{los}(t) = \exp\{j\pi FMt^2\} \cdot \exp\{-j\frac{4\pi}{\lambda}v_{los}t\} \tag{6}$$

The spectrum $T_{los}(f) = U_{los}(f) \cdot S(f)$ of the moving target after focusing with a SWMF results in

$$T_{los}(f) = \exp\left\{-j2\pi\frac{2fv_{los}}{\lambda FM}\right\}\exp\left\{-j2\pi\frac{2v_{los}^2}{\lambda^2 FM}\right\} \tag{7}$$

As one can see, $T_{los}(f)$ is composed of a linear phase (first part) and a constant phase term (second part). Following the laws of fourier transform the linear phase component corresponds to a *time shift t_{shift} in time domain*. Fourier-transforming the linear term of Eqn.(7) yields

$$t_{shift} = \frac{2v_{los}}{\lambda FM} \quad [s]. \tag{8}$$

Some simple transformations of Eqn.(8) give the *azimuth displacement of a moving object in space domain*

$$\Delta_{azimuth} = -R\frac{v_{los}}{v_{sat}} \quad [m] \tag{9}$$

with $t_{shift} = \frac{\Delta_{azimuth}}{v_B}$ here v_B is the beam velocity on ground. Across-track motion consequently results in an along-track displacement of the moving object. It is displaced in flight direction when the object moves towards the sensor (i.e. the range decreases) and reverse to flying direction when the movement is directed away from the sensor (i.e. the range increases).

Another effect caused by across-track motion is the introduction of a phase-shift in the SAR-Data. Since the phase of a conventional SAR-data is randomly distributed, this effect is of no use with a single SAR-Image. However if you can use two or more recordings like in along-track interferometry, that phase-shift can be useful. The phase-shift can be expressed as range difference ΔR in line-of-sight direction, which in turn is related to object motion

$$\psi = \frac{4\pi}{\lambda}\Delta R = \frac{4\pi}{\lambda}v_{los}t \tag{10}$$

When the time frame t is limited by the satellite motion and the distance Δl of the phase centers of the two antennas, Eqn.(10) can be reformulated as

$$\psi = \frac{4\pi}{\lambda}v_{los}\frac{\Delta l}{v_{sat}} \tag{11}$$

Since both, interferometric phase ψ and azimuth displacement $\Delta_{azimuth}$, are only caused by across-track motion, an analytic relation between both measurements can be established

$$\Delta_{azimuth} = -R\frac{v_{los}}{v_{sat}} = -R\psi\frac{\lambda}{4\pi\Delta l} \tag{12}$$

2.22 Along-track Motion The target is now assumed to move with velocity v_{x0} in azimuth direction (along-track). The relative velocity of sensor and scatterer is different for the moving object and the surrounding stationary world. Thus, along track motion changes the frequency modulation (FM) rate of the received scatterer response. Focusing the signal of a moving vehicle $u_{mt}(t)$ with the SWMF $s(t)$ in frequency domain yields

$$T_{mt}(f) = U_{mt}(f) \cdot S(f) = \exp\left\{-j\pi\frac{f^2}{\delta FM}\right\} \tag{13}$$

where

$$\frac{1}{\delta FM} \approx -\lambda\sqrt{\frac{v_{sat}}{v_B}}\frac{v_{x0}}{(v_{sat}v_B)^{\frac{3}{2}}}R \tag{14}$$

The phase of the focused signal $T_{mt}(f)$ is quardatic and causes a spreading of the signal energy in time or space domain depending on δFM. Unfortunately, the fourier transform of $T_{mt}(f)$ has no analytic solution. Nevertheless, considering the stationary phase approximation of the Fourier-Transform the width of the focused peak can be approximated by

$$\Delta t \approx \frac{PRF}{\delta FM} = 2T_A\frac{v_{x0}}{v_B} \quad [s] \tag{15}$$

with T_A being the aperture time. Interpretation of Eqn.(15) shows that *a moving vehicle is smeared by twice the distance it moved along-track during the illumination time T_A*. It has to be kept in mind that the approximation in Eqn.(15) only holds if $v_{x0} \gg 0$.

3. DETECTION METHODS

For detecting vehicles one can make use of the effects mentioned in Sect.2. In this paper will focus on detection methods making use of the effects causes by across-track motion. Along-track motion effects are dealt with in (Weihing *et al.* , 2006). There are two major methods to approach detection with across-track motion: along-track SAR interferometry (ATI), and SAR displaced phase center antenna (DPCA). Both make use of the phase-shift in order to detect vehicles. In a second step the displacement can be used to estimate the velocity of the vehicle.

3.1 ATI

In the case of along-track interferometry (ATI) an interferogram I_{ATI} is formed from the original complex data sets I_1 and I_2 by calculating

$$\begin{aligned} I_{ATI} &= I_1 \cdot I_2^* = |I_1|\,|I_2| \exp\left(j\left(\varphi_1 - \varphi_2\right)\right) = \\ &= \eta \exp\left(j\psi\right) \qquad (16) \\ \text{with} \quad & \varphi_1 = \arg\left(I_1\right) \text{ and } \varphi_2 = \arg\left(I_2\right) \\ \text{and with} \quad & \psi = \varphi_1 - \varphi_2 \qquad (17) \end{aligned}$$

For all stationary targets the interferometric phase values $\psi = (\varphi_1 - \varphi_2)$ will be statistically distributed around the expectation

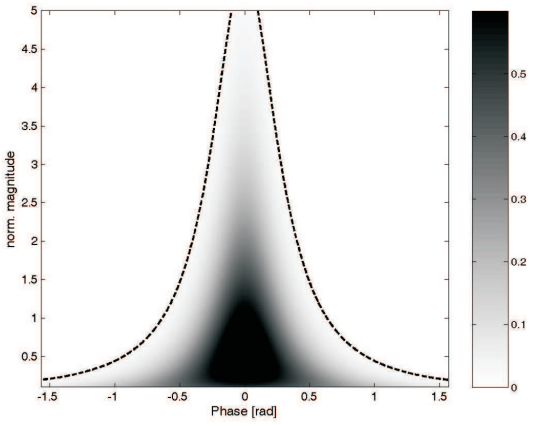

Figure 1. Theoretical joint probability density function $f_c(\eta, \psi)$ of the single-look interferometric phase and a magnitude normalized to $E[\eta] = 1$. Coherency is set to $|\rho| = 0.95$. The dashed line is an example for a curve of separation.

value $E[\psi] = 0$. The joint probability density function (pdf) $f_c(\eta, \psi)$ of amplitude and phase of an interferogram has been derived in (Lee *et al.* , 1994) and (Joughin *et al.* , 1994) using the underlying assumption of jointly Gaussian-distributed data in the two images. It is given by:

$$f_c(\eta,\psi) = \frac{2n^{n+1}\eta^n}{\pi\Gamma(n)\left(1-|\rho|^2\right)} \exp\left(\frac{2n\eta|\rho|\cos(\psi)}{1-|\rho|^2}\right) \cdot K_{n-1}\left(\frac{2n\eta}{1-|\rho|^2}\right) \quad (18)$$

where n is the number of looks, $\Gamma(\bullet)$ is the gamma function and $K_n(\bullet)$ is the modified Bessel function of the nth kind. As a precondition for the validity of the pdf it was assumed that $E\left[\eta^2\right] = 1$. Multilooking is done by averaging over n pixels assuming stationarity. For medium resolution SAR the jointly Gaussian assumption has been validated in most agricultural and heavily vegetated areas. Fig.1 shows a typical example of the pdf assuming a coherency of $|\rho| = 0.95$, $n = 1$ and a expected signal amplitude of $E[\eta] = 1$.
Fig.1 illustrates the typical behavior of the clutter that large phase fluctuations are associated with small amplitudes (destructive interference in the speckle patterns of the images). The phase variations are drastically reduced for large amplitudes (constructive interference in the speckle patterns of the images). The pdf is centered on a phase value of $\psi = 0$ as expected.
Based on this pdf a constant false alarm rate (CFAR) detector can be designed that groups all image pixels into two classes. Class 1, called 'clutter only', contains all pixels that only carry image information. Class 2, called 'no clutter', contains all pixels that are not part of the image pdf. This class 2 includes pixels that contain moving vehicles but also all sort of outliers. Classification is done by comparing that pdf with thresholds α. This provides us with a curves of separation between the two classes, which are actually isolines on $f_c(\eta, \psi)$. An example of a possible curves of separation is indicated in Fig.1 by black dashed lines. The chosen curve of separation determines the probability of false alarm (P_{fa}); sometimes also referred to as "'false alarm rate"' (FAR). It is simply the integral of the Clutter pdf over the area where $f_c(\eta, \psi) < \alpha$. Thus, the FAR describes the rate of 'clutter only' pixels that are wrongly assigned to the class 'no clutter'.
To implement a CFAR-Detector, several steps have to be accomplished: First the ATI-Image I_{ATI} has to be computed. As mentioned earlier expected signal amplitude of the pdf in Eqn.(18) is $E[\eta] = 1$. The SAR data used might not have that property. So it is necessary apply some normalization. Additionally the coherence as a parameter of Eqn.(18) has to be determined. Then, for each pixel the value of the pdf can be computed. Inputs are the phase and magnitude of I_{ATI} and the coherence. Finally a threshold is applied to decide whether a pixel is Class 1 ('clutter only') or Class 2 ('no clutter').

3.2 DPCA

In a similar way, detection using DPCA is accomplished. First a coherent difference I_D of the original complex data sets I_1 and I_2 is computed:

$$I_D = I_1 - I_2$$

Ideally this would results in a complete removal of the clutter. What remains is only noise introduced by the receiver and signal from the vehicle (if present). Hence a pixel of class 1 ('clutter') would only contain receiver noise and its distribution would be complex circular gaussian:

$$f_D(I_D) = \frac{1}{2\pi\sigma_D^2}\exp\left(-\frac{1}{2}\frac{\left(I_D^{(re)}\right)^2+\left(I_D^{(im)}\right)^2}{\sigma_D^2}\right) \quad (19)$$

$$\text{with } I_D = I_D^{(re)} + jI_D^{(im)}$$

In reality the two antennas have different characteristics which can result e.g. in a remaining phase ramp or in imbalances in magnitudes of the two channels. Hence some sort of preprocessing is often necessary to balance the channels. For possible methods see (Gierull, 2003) or (Ender, 1996) for further reference. As detection using ATI benefits from this kind of preprocessing as well it is advisable to apply it to all data as an independent step in the processing chain before the actual detection. (The steps of the processing chain will be dealt with in Sect.5.1) The procedure for detection with DPCA is similar to that with ATI: As in the case of ATI a normalization has to be conducted. For that the variance σ_D^2 is computed. Since the characteristics of the SAR data can change over azimuth and range, this cannot be done globally, but has to be done locally using a using a sliding window method. Together with the pixel values of I_D, σ_D^2 is input to Eqn.(19) as a parameter. Then, for each pixel the value of the pdf is computed. Again the final step is to apply a threshold to decide whether a certain pixel images clutter or a vehicle.

4. SIMULATION

4.1 Parameters of interest

In order to obtain an estimate on the detection performance, with no satellite data available so far, monte-carlo simulations were conducted. In these simulations the most important properties of the satellite, the moving vehicle and the background of the vehicle were incorporated. The satellite is characterized by various parameters such as bandwidth, antenna-pattern, ATI baseline. Clutter also differs depending on whether forest, grassland or an urban area is imaged. And finally the moving vehicle has to be characterized adequately as well. Here it is modeled as a point-target, but even then the RCS and the velocity in line-of-sight have to be considered in the simulation. Sensor parameters were set to match TerraSAR-X specifications. See table (Meyer *et al.* , 2005) for a list of the most important parameters.

All these facts can be merged in the following parameters:

- resolution of the radar image: δx, δr
- radar-crossection (RCS)of the vehicle: σ_V
- relative radar-crossection of the clutter: σ_C^0
- noise-equivalent sigma zero (NESZ): σ_{NESZ}^0
- across-track velocity v_r of the vehicle considered, corresponding to the phase shift ϕ introduced in the SAR-data

Resolution and NESZ only depend on the satellite and were fixed in all simulations. On the contrary the RCS of the vehicle, vehicle velocity and RCS of the clutter had to be varied to accommodate different simulation scenarios.

4.2 Simulating Data

For the simulation two sets of random samples are created. Each sample consists of two complex numbers, resembling the two channels of the SAR-System. One set I^C was simulated to contain clutter only, the other set I^V to contain the radar return of a vehicle embedded in clutter. To compute these two sets first six sets of complex gaussian distributed random samples are generated. (see Eqn.(20)).

$$R_y^x = \mathcal{N}(0,1) + j\mathcal{N}(0,1) \tag{20}$$

Then, with the use of Eqn.(22) to Eqn.(24) the two sets I^C and I^V are computed.

$$I_1^C = \sigma_C^0 R_1^C + \sigma_{NESZ}^0 R_1^N \tag{21}$$
$$I_2^C = \sigma_C^0 R_1^C + \sigma_{NESZ}^0 R_2^N \tag{22}$$
$$I_1^V = \frac{\sigma_V}{\delta x \delta r} + \sigma_C^0 R_2^C + \sigma_{NESZ}^0 R_3^N \tag{23}$$
$$I_2^V = \frac{\sigma_V}{\delta x \delta r} e^{j\phi} + \sigma_C^0 R_2^C + \sigma_{NESZ}^0 R_4^N \tag{24}$$

In order to obtain good statistics the number of elements in each set has to be very high. In our case 10000000 elements per set were used. These two sets are then put into the detector. With the result from I^C the false alarm-rate P_{FA} is computed, by dividing the number of samples falsely detected as vehicles over the total number of samples. Similarly, with the set I^V, the probability of a missed vehicle P_M and the probability of detecting a vehicle P_D are computed.

4.3 Results of the Simulation

SAR-Data has statistical properties, hence the need for a monte-carlo simulation. Statistical fluctuations have an influence on the SAR-Image in different ways: The radar-crossection (RCS)of the vehicle varies depending on the aspect-angle of the vehicle. The Clutter itself has statistical fluctuations. And additionally the receiver of the radar-system adds a noise-floor to the obtained image. So an accidentally bright clutter-pixel could be brighter than an pixel imaging a vehicle in an unfavorable aspect angle. In such an unfavorable situation the receiver-noise could also introduce a phase-shift to the data which could be higher than the one of a slow vehicle. As one can see there is always a trade-off between the number of vehicles missed (missed hits) and the number of false alarms i.e. clutter which is falsely detected as a target.
To show this trade-off one can plot th P_{FA} against the P_M, or equivalently the P_{FA} against P_D, since $P_D + P_M = 1$. Such a plot is called a ROC-Curve, an example is is depicted in Fig.2.

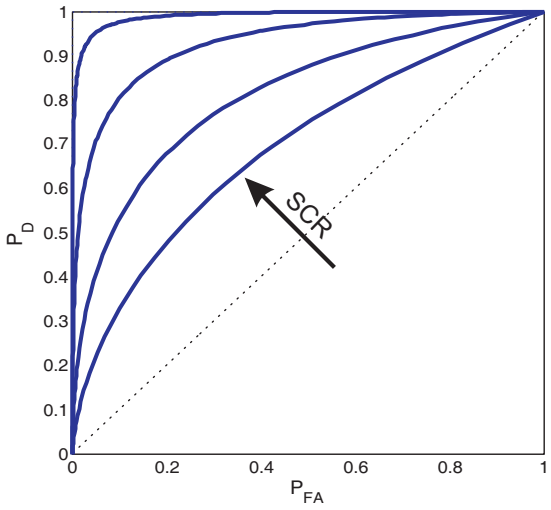

Figure 2. Performance of an DPCA-detector for signal to clutter ratios of -3dB, 0dB, 3dB, 6dB and 10dB (innermost to outermost).

For an ideal detector, the ROC-curve would jump up to a probability of detection of 1 right away, holding $P_D = 1$ for any P_{FA}. The worst case - a detector just guessing - is indicated by the thin dashed line.
This kind of view is useful in showing the quality of an detector, however it is hard to show the dependence of the detector on other parameters. In Fig.2 this is done by plotting several ROC-Curves in the same plot. But it gets very complex and counter intuitive.

For further plots therefore only the values of P_D for a fixed P_{FA} are plotted against various parameters, which have an influence on the performance of the detector. Fig.3 and Fig.6 show examples of such plots. Here the P_D of the target is plotted against the RCS of the vehicle for the across-track velocities of 50 km/h, 80 km/h and 150 km/h. The False-Alarm Rate P_{FA} in that example and in all of the following examples is fixed at $P_{FA} = 10^{-4}$. In Fig.3 detection with DPCA was simulated; Fig.6 shows detection with ATI. As one can see with DPCA there is an interval of about 8 dBm^2 where the probability of detection increases from 0 to 1. With ATI that interval is a bit larger, about 10 dBm^2. Clearly, the position of the interval varies depending on the method of detection and the mainly the velocity of the vehicle. To point out the dependence of the P_D on both the velocity and the RCS of the vehicle Fig.4 and 7 show a similar plots, here P_D is ploted against both parameters.
For the previous simulations a constant RCS was assumed. However in reality the RCS of a vehicle is randomly distributed rather than fixed at a deterministic value. Another simulation was conducted to accommodate that fact. In Fig.4.4 and Fig.4.4 the P_D for vehicles are shown where the RCS is gaussian distributed with a standard deviation of 8 dbm^2 and a mean values ranging from 0 dbm^2 to 11 dbm^2.

4.4 Conclusions from Simulation

On the whole DPCA performs better for high and medium valued velocities while ATI has an advantage for small valued velocities. That advantage is mainly due to the fact, that with ATI one can incorporate the vehicle's amplitude while with DPCA the vehicle's amplitude is lost, if there is no or only a small phase-shift due to the vehicle's small velocity. This is true for both a deterministic and a randomly distributed RCS. Hence it is advisable to use both ATI and DPCA for detection and fuse the results to combine the advantages of both methods.

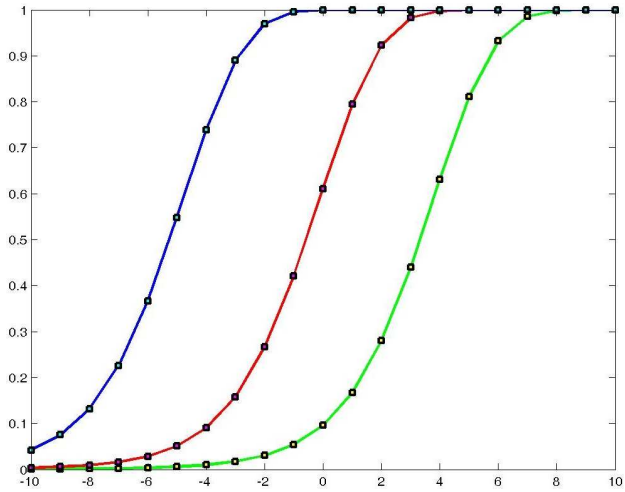

Figure 3. Plot of P_D for a DPCA-Detector against the RCS of a simulated vehicle

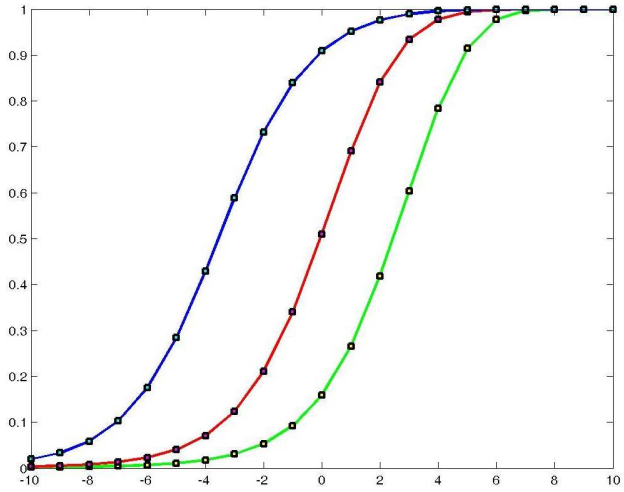

Figure 6. Plot of P_D for an ATI-Detector against the RCS of a simulated vehicle

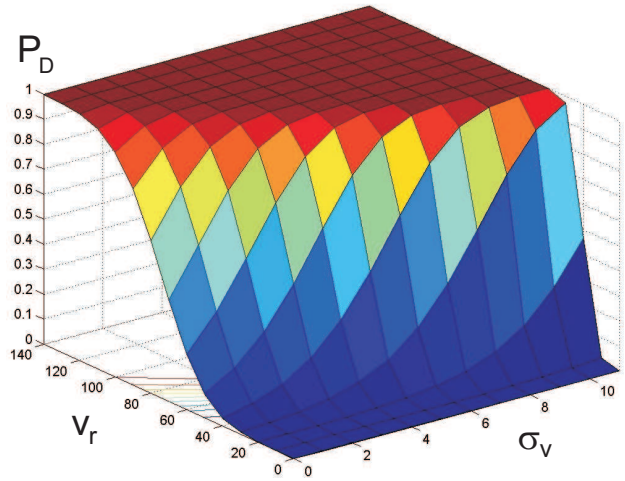

Figure 4. Plot of P_D for a DPCA-Detector against the RCS and velocity of a simulated vehicle

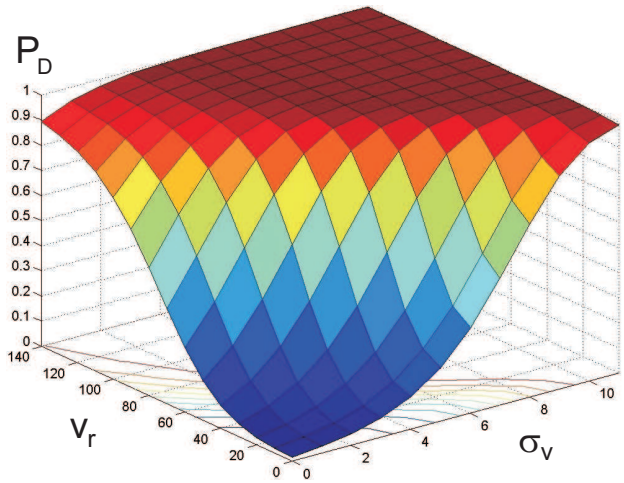

Figure 7. Plot of P_D for an ATI-Detector against the RCS and velocity of of a simulated vehicle

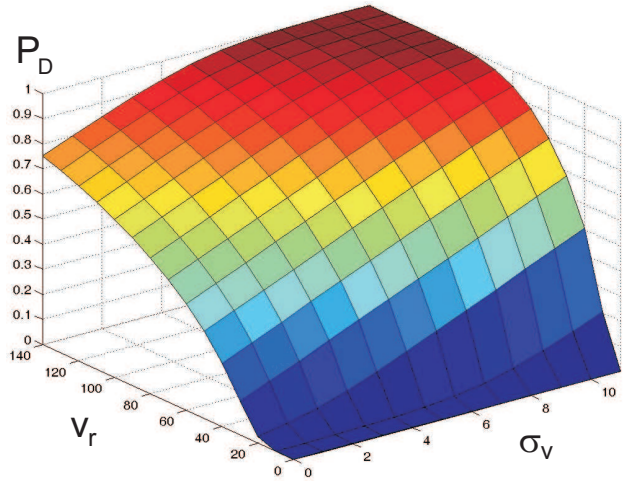

Figure 5. Plot of P_D for an DPCA-Detector against the a distributed RCS and velocity of of a simulated vehicle

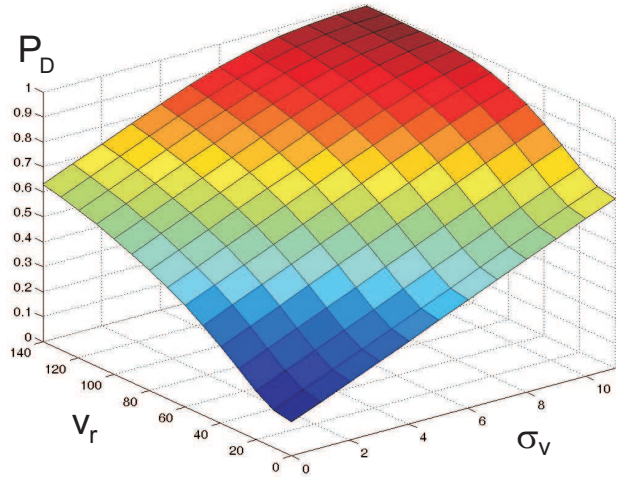

Figure 8. Plot of P_D for an ATI-Detector against the a distributed RCS and velocity of of a simulated vehicle

5. PROCESSING SAR DATA FOR TRAFFIC MONITORING

5.1 The traffic-processor

For a traffic-processor the methods described in Sect.3. have to be implemented. Furthermore additional steps before and after the actual detection are necessary. These steps are:

- SAR processing of the raw data:
  The conventional SAR processing steps such as focusing of the raw data or squint processing for air-borne data have to be conducted
- Channel Ballancing:
  The magnitudes and phases of the two SAR-images have to be adapted to each other. Magnitudes should have the same level and potential phase-ramps have to be removed. See e.g. (Gierull, 2003) for further reference.
- Detection with ATI or DPCA:
  Detection Algorithms specified in Sect.3. are applied here.
- Estimation of vehicle velocity from displacement:
  Knowledge about the road-network of the scene imaged is imported through a GIS-database. With that knowledge, the displacement and heading direction of the vehicles can be determined. Thereby the velocity of the vehicles is determined.

The traffic-processor was developed at DLR and is currently used to process SAR-Data from DLR's airborne ESAR-System. The experience gained with this experimental system will later be used to construct a traffic-processor for TerraSAR-X data.

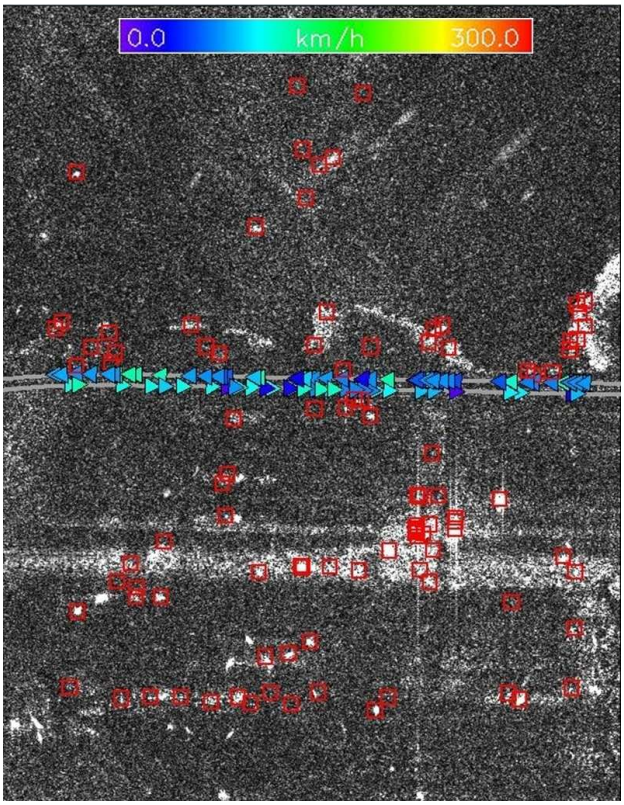

Figure 9. Result of the traffic-processor showing detected vehicle and their back projection onto the road

5.2 Results with the traffic-processor

In Fig.9 a result of the traffic-processor is shown. The scene imaged is the "'Autobahn"' A8 at lake Chiemsee. Vehicles detected are marked with red squares. Additionally the track of the "'Autobahn"' is superimposed onto the image. The vehicle's true position is marked by triangles. Those were color-coded according to the estimated velocity. Higher order parameters like the density of the vehicles and the estimated time to pass a certain section of the road are expected to be computable from those results. Another flight campaign is going to be conducted where not only SAR-data will be recorded but also optical images will be taken, so that the results from radar-data can be compared with another source of information to learn more about the reliability of SAR-data.

REFERENCES

Bamler, R. and Schättler, B., 1993. *SAR geocoding*, Chapter 3, pp. 53–102. Karlsruhe: Wichmann.

Breit, H., Eineder, M., Holzner, J., Runge, H., and Bamler, R., 2003, jul). Traffic Monitoring using SRTM Along-Track Interferometry. In *IGARSS*.

Cumming, I. and Wong, F., 2005. *Digital Processing of Synthetic Aperture Radar Data*. Boston: Artech House.

Ender, J., 1996. The airborne experimental multi-channel SAR system AER-II. In *EUSAR96 Conference*, Königswinter, Germany, pp. 4952.

Gierull, C. H., 2001, jul). Statistics of SAR interferograms with application to moving target detection. Technical Report DREO-TR-2001-045, Defence R&D Canada.

Gierull, C. H., 2002, aug). Moving Target Detection with Along-Track SAR Interferometry. A Theoretical Analysis. Technical Report DRDC-OTTAWA-TR-2002-084, Defence R&D Canada.

Gierull, C. H., 2003, mar). Digital channel balancing of along-track interferometric sar data. Technical Report DRDC-OTTAWA-TM-2003-024, Defence R&D Canada.

Joughin, I., Winebrenner, D., and Percival, D., 1994, may). Probability density functions for multilook polarimetric signatures. *IEEE Transactions on Geoscience and Remote Sensing* 32(3), 562–574.

Klemm, R., 1998. *Space-time adaptive processing*. London, United Kingdom: The Institute of Electrical Engineers.

Lee, J.-S., Hoppel, K., Mango, S., and Miller, A., 1994, sep). Intensity and phase statistics of multilook polarimetric and interferometric SAR imagery. *IEEE Transactions on Geoscience and Remote Sensing* 32(5), 1017–1028.

Meyer, F., Hinz, S., Laika, A., and Bamler, R., 2005. A-priori information driven detection of moving objects for traffic monitoring by spaceborne SAR. In *Proceedings of ISPRS-Workshop CMRT 05 "City Models, Road Databases, and Traffic Monitoring - Concepts, Algorithms, and Evaluations*, Vienna.

Weihing, D., Hinz, S., Meyer, F., Laika, A., and Bamler, R., 2006. Detection and along-track velocity estimation of ground moving targets in high resolution spaceborne SAR images. In *ISPRS Mid-Term Symposium: "From Pixels to Processes"*.

ACKNOWLEDGEMENTS

This work has been founded by the DLR project "'TerraSAR-X Traffic Products"'. Special Thanks to the project members Hartmut Runge, Gintautas Palubinskas and Michael Eineder for their support.